



# Plug-and-play radiation sensor components for unmanned aerial system platform

Monia Kazemeini<sup>1</sup> · Zachary Cook<sup>1</sup> · Joon Lee<sup>1</sup> · Alexander Barzilov<sup>1</sup> · Woosoon Yim<sup>1</sup>

Received: 29 April 2018 / Published online: 6 October 2018  
© Akadémiai Kiadó, Budapest, Hungary 2018

## Abstract

Mobile radiation sensing techniques for surge deployment and wide area search are important for nuclear security applications. Radiation sensors were developed for the use with robotic platforms of unmanned aerial systems (UAS). Ambient temperature neutron and gamma CLYC sensor and high resolution CZT gamma sensor were integrated into the UAS as plug-and-play interchangeable components allowing easy attachment to a robot in field conditions. The time and position data were added via Robot Operating System to measured intensities of photon peaks and neutron rates enabling the input for the UAS flight control. The contour mapping of a radiation area by multiple UAS was simulated.

**Keywords** Unmanned aerial system · CLYC · CZT · Plug-and-play components · Radiation monitoring · Robot Operating System

## Introduction

Radiation detection technologies are vital for radiological safety and nuclear security applications. Radiological and nuclear materials can be displaced, lost, smuggled [1], or released into the environment due to accidents such as the Fukushima Daiichi nuclear power plant accident [2]. The use of small scale unmanned aerial systems (UAS) enables remote radiation sensing and mapping and wide area search operations by keeping humans away from the risk of exposure. Multi-use UAS platforms equipped with navigational and radiation sensing capabilities enable performing surveillance in hard to reach, hazardous areas, allowing the measurements to be dynamically tracked and mapped. The measured data could be used for further analysis in temporal and space domains. Furthermore, based on the cooperative sensing algorithms, the UAS swarm can be programmed to search for unattended radiation sources.

The gamma and neutron radiation sensors integrated into the UAS platform are required. The choice of the radiation detector is important for the UAS due to the fact that flying efficiency is reduced when there is an increase in payload. These sensors should be easily attached to the UAS in field conditions. Radiation sensors should be lightweight and low power so that they can be integrated into the robotic platform without affecting data processing limitations, payload, or battery power. To address this need, two flight-ready ambient temperature radiation sensors were developed as plug-and-play interchangeable components: the Cadmium Zinc Telluride (CZT) sensor for high-resolution gamma spectrometry, and the Cs<sub>2</sub>LiYCl<sub>6</sub>:Ce<sup>3+</sup> (CLYC) sensor for simultaneous neutron and gamma measurements.

## CZT sensor

A CZT sensor was designed as an onboard module for high resolution gamma ray measurements. CZT is a room temperature, wide bandgap semiconductor that directly converts photons into charge carriers. These semiconductors are able to process more than ten million photons per square millimeter per second. A Kromek GR1-A unit [3] was used for the integration into a multicopter UAS. The

✉ Alexander Barzilov  
alexander.barzilov@unlv.edu

<sup>1</sup> Department of Mechanical Engineering, University of Nevada, Las Vegas, 4505 S. Maryland Parkway, Las Vegas, NV 89154-4027, USA

GR1-A has a  $1 \text{ cm}^3$  CZT and is powered via USB; the USB is used for the data communication as well. The power consumption of the sensor is about 250 mW. The unit is lightweight, making it ideal for the mounting on the platform. The unit's volume is  $(2.5 \times 2.5 \times 6.1) \text{ cm}^3$  and its weight is about 50 g.

The sensor's energy range is from 30 keV to 3 MeV with an energy resolution of less than 2% at 662 keV. The temperature range is from 0 to 40 °C. Figure 1a, b shows the GR1-A module and the CZT sensor being mounted onto the UAS platform—the octocopter DJI S1000+.

A block diagram of the CZT sensor operation is shown in Fig. 2. Electric signals generated by the CZT crystal in proportion to energy of the incident gamma ray, are amplified by a preamplifier, and then processed by a shaping amplifier. A 4096 channel analyzer then generates the gamma ray spectrum file that can be further analyzed.

The Robot Operating System (ROS) [4] was used for the data fusion and communication. ROS is an open source tool, consisting of libraries used for robot applications. It is able to include any number of independent nodes, which communicate with each other, using a publishing/subscribing message to topics. Once the sensor's data file was sent via USB to an onboard Linux Odroid minicomputer and processed using the ROS installed on it, a gamma ray spectrum is formed. Figure 3 shows the measured spectra of  $^{137}\text{Cs}$  and  $^{60}\text{Co}$  sources. The data acquisition time can be set by the user or the control software.

Automated methods are widely used for the gamma spectrum analysis, for example wavelet based techniques [5]. For rapid spectral analysis in UAS applications with limited onboard computing resources, a robust, simple method is required. The Mariscotti's technique [6] was utilized for the automatic identification of peaks in the presence of a background. It enables to distinguish the full energy peaks from the Compton shoulders. In this technique, peaks are described by Gaussian function, and the

background is approximated by a linear function within a small region (several peak widths). In such small interval, the number of counts as a function of the channel  $i$  is approximated as  $y(i) = G(i) + C_1 + C_2i$ , where  $G(i)$  is Gaussian function if a peak exists or zero if not;  $C_1$  and  $C_2$  are constants describing the background. The technique locates a peak where a second derivative of  $y(i)$  is not zero.

The Gaussian is  $G(i) = A \exp\left(-\frac{(i-p)^2}{2\sigma^2}\right)$ , where  $A$  is the intensity of the peak centered at channel  $p$ ,  $\sigma = FWHM_{peak}/2.355$ . For discrete data, the second derivative was replaced by a second difference  $S(i) = y(i+1) - 2y(i) + y(i-1)$ . Because  $y(i)$  has a statistical error,  $S(i)$  will have statistical fluctuation about expected values based on their standard deviation; therefore, if the expected  $S(i)$  value at  $i = p$  is similar to the standard deviation, a peak cannot be located. For  $\sigma = 4$  it yields  $A = 600$ . In order to resolve smaller peaks, the function  $S(i)$  was replaced by its "smoothed" form, reducing the standard deviation. The smoothed second difference is an average of  $S(i)$  values over  $w$  neighboring channels around the channel  $i$ ; this process can be repeated. As shown in [6], the generalized second difference averaged  $z$  times over  $w$  channels around  $i$  can be approximated as  $S_i(z, w) = \sum_j C_{ij}(z, w)y_j$ , where  $C_{ij}$  represent the weighting factors, and its standard deviation is  $D_i(z, w) = \left[\sum_j C_{ij}^2(z, w)y_j\right]^{1/2}$ . The parameters  $z$  and  $w$  were chosen for the detector based on the desired minimum for  $A$  value.

The exact position of the peak was identified at the center of the Gaussian. The area underneath the peak was used for the calculation of the peak's intensity. This algorithm was written using C language within the ROS. Each spectrum file was processed automatically, and only the intensities and energies of found peaks were transmitted to the user, thus minimizing the data streams.

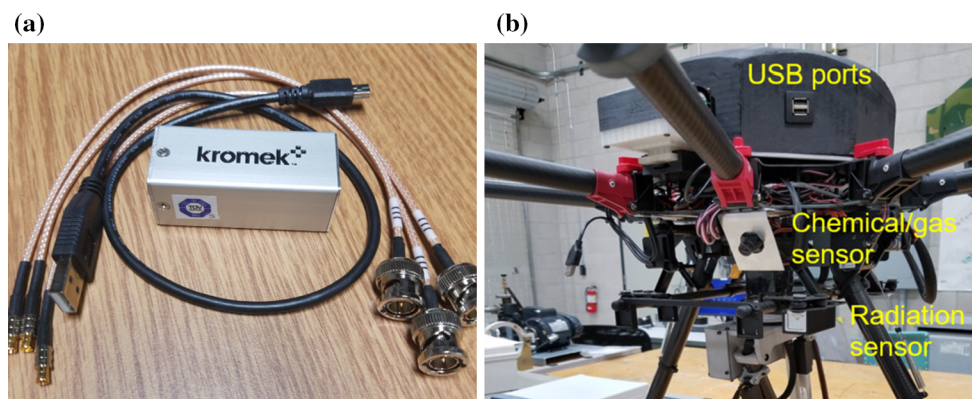


Fig. 1 a GR1-A CZT module; b CZT sensor mounted on UAS platform

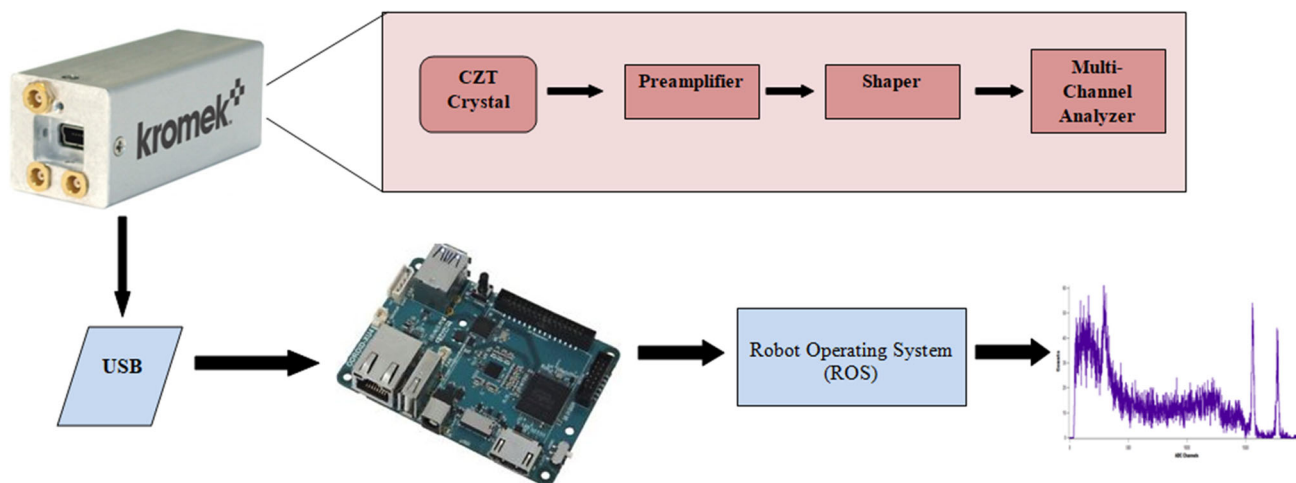
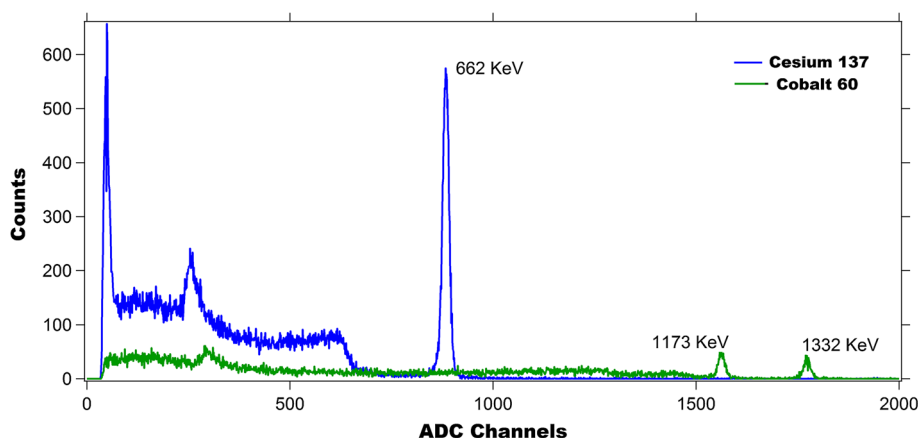


Fig. 2 Block diagram of CZT sensor operation

Fig. 3 Gamma ray spectra of  $^{137}\text{Cs}$  and  $^{60}\text{Co}$  sources



## CLYC sensor

The 1-inch diameter, 1-inch long elpasolite CLYC [7] scintillator crystal was used to design the compact neutron/gamma sensor for the UAS. It allows for an ambient temperature photon spectrometry that showed suitable scintillation properties. The CLYC crystal was coupled with a PMT, a miniature eMorpho digitizer, and a high voltage generator, then packaged in the housing (see Fig. 4a). The energy resolution was measured to be 5% at 662 keV, 3.6% at 1173 keV, and 3.3% at 1332 keV. It has a density of  $3.31 \text{ g/cm}^3$  and a spectral range of 275 nm to 450 nm. The refractive index is 1.81. The scintillation light yield is 20,000 photons/MeV for gamma rays and 70,000 photons/neutron for thermal neutrons. The CLYC's lithium-6 enrichment is 95%; it enables neutron detection via the  $^6\text{Li}(n,\alpha)t$  reaction.

CLYC has pulse shape discrimination (PSD) properties. The fast core-to-valence (CVL) and a prompt  $\text{Ce}^{3+}$  decay follow a gamma-ray induced event in CLYC (1 ns and 50 ns decay constants, respectively). Neutron induced

events in CLYC are followed by a slow cerium self-trapped excitation (Ce-STE) with the 1000 ns decay constant [8]. Figure 4b shows the digitized CLYC waveforms of the neutron and photon signals.

Each waveform was processed on the fly using a digitizer, yielding three values saved in the list mode: an integral under the 'front' part of the signal calculated during the preset partial integration time, the 'total' integral, and the time value captured when the signal amplitude exceeded a threshold. The PSD value was calculated for each signal as  $(total\ integral - front\ integral)/front\ integral$ . The neutron signals with longer tails provide larger PSD values compared to photon signals. This PSD method allowed for distinguishing of the signals that were obtained from the photon and neutron interactions. Figure 4c shows the experimental data of the neutron/photon PSD for the CLYC sensor using a 2 Ci PuBe source. Figure 4d shows PSD properties of the CLYC: neutron and gamma signals are well separated. The PSD figure of merit  $FOM = T/(W_1 + W_2)$  was calculated to be about 2.3.

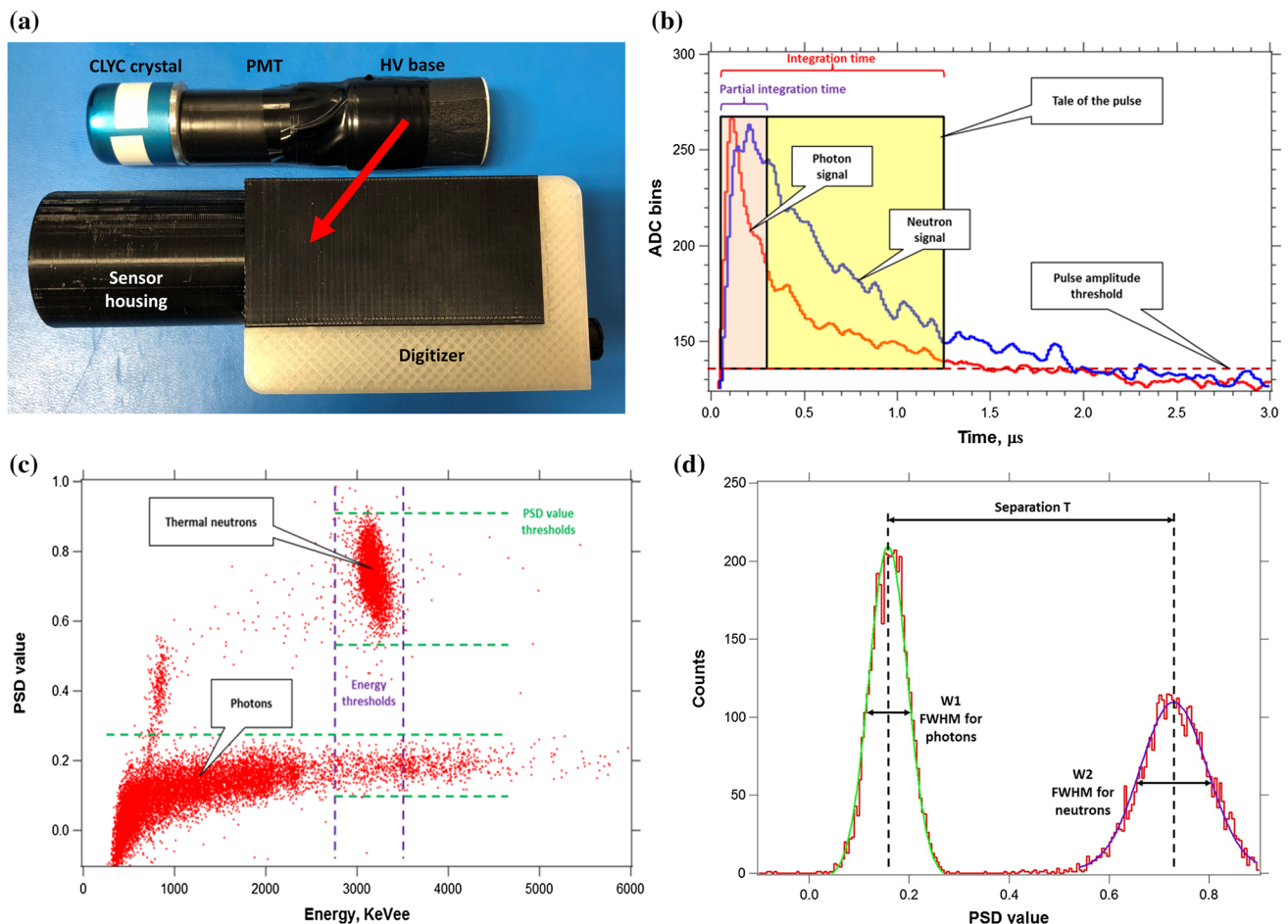


**Fig. 4** **a** CLYC sensor module; **b** signal waveforms; **c** CLYC neutron/photon PSD; **d** figure of merit of PSD using a PuBe source

## Plug-and-play interchangeable sensor components

Plug-and-play concept was used to integrate the radiation sensors into the UAS via ROS. This supports 'hot plugging' of the sensor into the UAS platform, meaning that the user does not need to set up component's parameters each time the UAS is powered on. Each time a component is plugged, the operating system recognizes the component, then it installs a device driver to read and process the sensor's data. The data is then published and the message appears. Likewise, when the sensor is unplugged, the operating system removes the device driver and the process is terminated. An operational block diagram is shown in Fig. 5. Figure 6 illustrates testing the plug-and-play operation of the CLYC sensor.

## Application of UAS based radiation sensors

The developed sensors enable fusion of measured and processed onboard radiation data (energies of gamma-ray peak centroids and their intensities for the CZT sensor; neutron rates and energies of gamma-ray peak centroids and their intensities for the CLYC sensor) with the GPS coordinates and time stamps of each measurement. The cooperative sensing algorithms that share information with multiple robotic platforms of the UAS swarm [9–11] require such fused data. Moreover, ROS enables the use of the sensor data in the control of a single UAS motion.

The algorithm for radiation source localization and contour mapping was implemented for three UAS that are positioned in a rotating circular formation (Fig. 7). This formation was shown as an effective swarm for mapping of large areas in [9, 10]. Each of the UAS carries a radiation sensor, thus they measure radiation simultaneously in three locations. It allows estimating the average count rate at the center of the circular UAS formation using their sensor's

Fig. 5 Block diagram of the plug-and-play operation

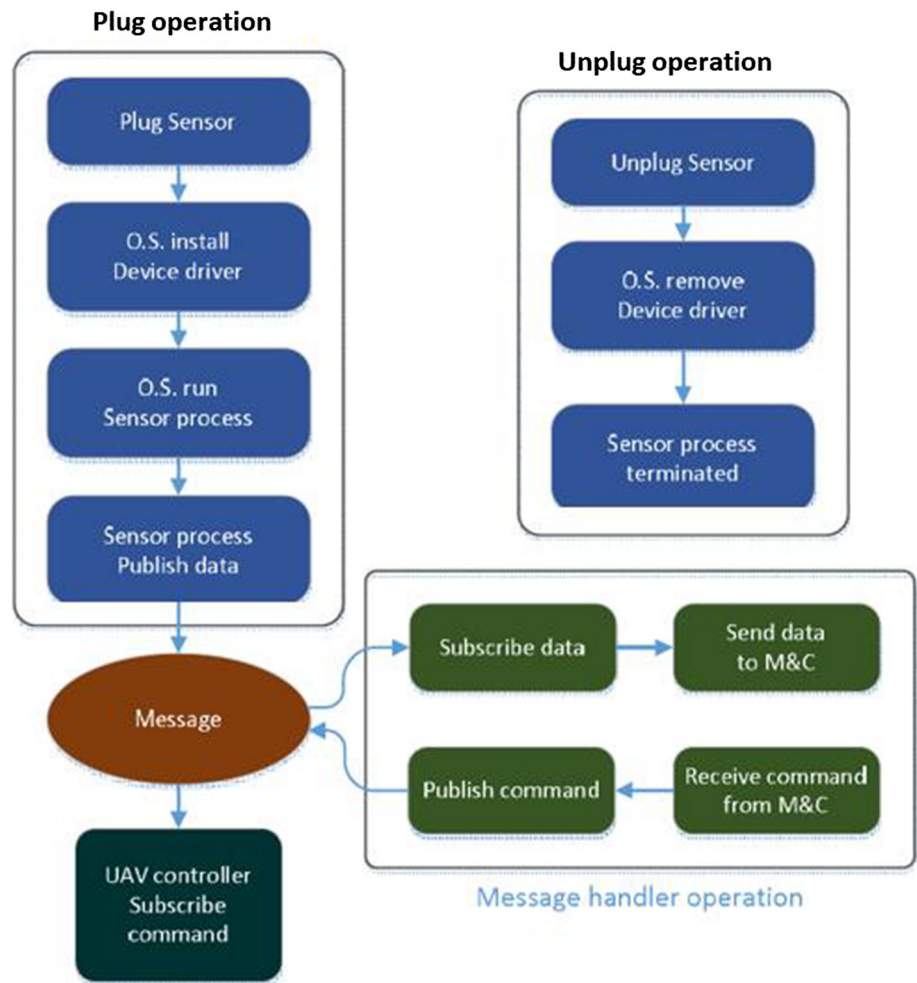
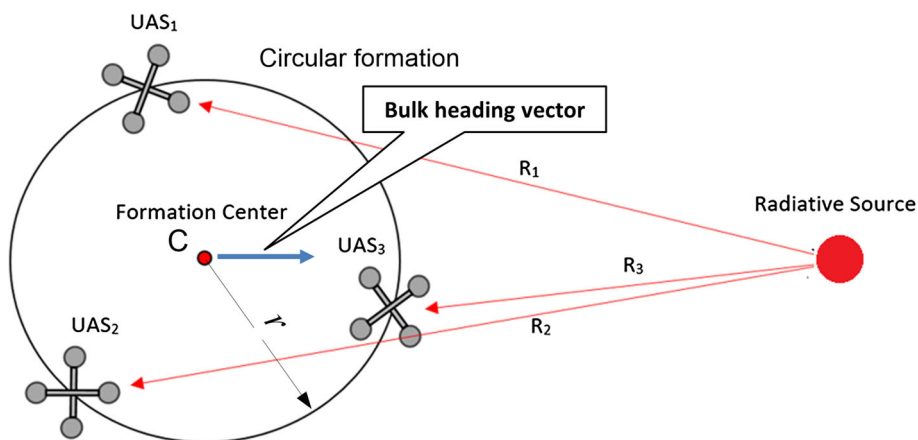


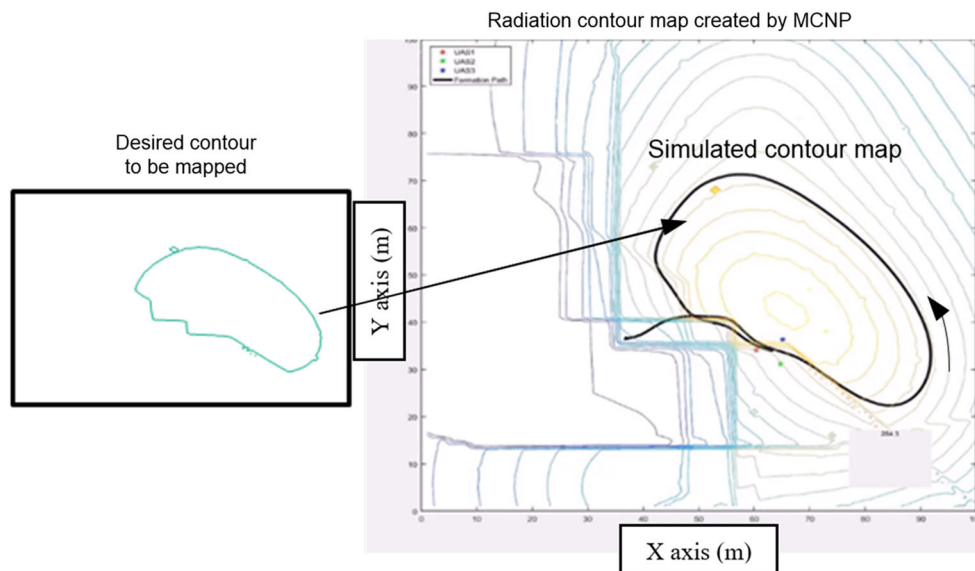
Fig. 6 Test of the plug-and-play operation of a CLYC sensor



**Fig. 7** Three UAS in a circular formation



**Fig. 8** Simulated contour mapping



readings. This approach is based on the estimation of the signal change to determine the steepest gradient direction which governs a bulk heading vector (for the center of the swarm) to follow. The source-seeking behavior is accomplished by directing the swarm toward the most increasing gradient. To map the reference contour, swarm should move tangentially to the radiative signal field. Contour mapping based on the preset values of intensities of specific gamma-ray peaks (that can be expressed in dose values) provides a precise boundary of the safe area for human exploration.

The algorithm includes UAS dynamics and adaptive spinning of the swarm for a reduced flight trajectory of each UAS platform. The swarm control algorithm was evaluated in a computational model using a computed photon distribution in a volume for the automatic following of a contour with the preset value of the photon flux at a given energy. MCNP6 code [12] was used for modeling of the photon flux in the volume of dimensions 100 m by

100 m by 16 m that contained five gamma-ray sources (3 MeV to 6 MeV). The concrete building was used in the model. A reference contour to be mapped is shown in Fig. 8 on the left. The swarm's initial position was located inside the field. The algorithm enabled mapping the reference contour within  $\pm 0.5$  m.

## Conclusion

Two radiation sensors were developed for unmanned aerial system platforms for the field applications. Ambient temperature CZT and CLYC sensors were integrated onto the UAS as plug-and-play components. The CLYC sensor enables simultaneous neutron and gamma measurements including neutron/photon pulse shape discrimination with figure of merit 2.3. The CZT sensor allows high-resolution gamma spectroscopy with automated spectral analysis locating peaks and calculating their intensities. USB

hardware connections were used for both sensors to bridge the sensors and the main controller using the UAS power source, and ROS was used for data communication. To streamline the process of bridging disparate components into a cohesive network, the collection of libraries describing the publisher/subscriber communication of ROS nodes was developed for these sensors. The sensor's design supports hot-plugging, and does not require a system restart.

This technology provides the capability to readily add/replace sensor components to enable extensive condition measurement and greatly improve situation awareness and event management. The robotic and intelligent nature of the UAS based search and mapping system allows long-term measurements to be performed at desired locations to prevent disasters and reduce dose risks to people and infrastructure.

**Acknowledgements** This work is supported by the grant from Savannah River Nuclear Solutions, LLC under Contract No. 0000217400.

## References

1. Runkle R, Bernstein A, Vanier P (2010) Securing special nuclear material: recent advances in neutron detection and their role in nonproliferation. *J Appl Phys* 108:111101
2. Nagatani K et al (2013) Emergency response to the nuclear accident at the Fukushima Daiichi nuclear power plants using mobile rescue robots. *J Field Robot* 30(1):44–63
3. Kromek detect image identity (2017). <https://www.kromek.com/index.php/products/applications/radiation-detection/gr1-gamma-rayspectrometer>. Accessed 10 Apr 2018
4. Robot Operating System. <http://www.ros.org>. Accessed 2 Apr 2018
5. Barzilov A, Kessler B, Womble P (2015) Analysis of 14-MeV neutron induced gamma-ray spectra using multiwavelets. *Rad Meas* 79:43–49
6. Mariscotti M (1967) A method for automatic identification of peaks in the presence of background and its application to spectrum analysis. *Nucl Instrum Methods* 50(2):309–320
7. Giaz A et al (2016) The CLYC-6 and CLYC-7 response to gamma-rays, fast and thermal neutrons. *Nucl Instrum Methods A* 810:132–139
8. D'Olympia N et al (2013) Pulse-shape analysis of CLYC for thermal neutrons, fast neutrons, and gamma-rays. *Nucl Instrum Methods A* 714:121–127
9. Han J, Chen Y (2014) Multiple UAV formations for cooperative source seeking and contour mapping of a radiative signal field. *J Intell Robot Syst Theory Appl* 74:323–332
10. Arranz L, Seuret A, De Wit C (2009) Translation control of a fleet circular formation of AUVs under finite communication range. In: *Proceedings of IEEE conference on decision and control*, pp 8345–8350
11. Hartman J, Barzilov A, Novikov I (2015) Remote sensing of neutron and gamma radiation using aerial unmanned autonomous system. In: *2015 IEEE nuclear science symposium and medical imaging conference (NSS/MIC)*, pp 1–4
12. Goorley T (2012) Initial MCNP6 release overview. *Nucl Technol* 180(3):298–315